Folding of a Small RNA Hairpin Based on Simulation with Replica Exchange Molecular Dynamics

Guanghong Zuo,[†,‡] Wenfei Li,[*,‡] Jian Zhang,[‡] Jin Wang,[§] and Wei Wang[*,‡]

T-Life Research Center, Department of Physics, Fudan University, Shanghai 200433, China, National Laboratory of Solid State Microstructure and Department of Physics, Nanjing University, 210093, China, and State Key Lab of Pharmaceutical Biotechnology, Nanjing University, Nanjing 210093, China

Received: May 16, 2009; Revised Manuscript Received: December 8, 2009

The folding of a small RNA tetraloop hairpin is studied based on intensive molecular dynamics simulation, aiming to understand the folding mechanism of this small and fast RNA folder. Our results showed that this RNA hairpin has very complicated folding behavior in spite of its small size. It is found that the folding transition has low cooperativity. Instead of a two-state folding, four major states are observed, including the native state, the intermediate, the unfolded state, and the misfolded state. The misfolded state is mainly stabilized by the non-native hydrogen bonds, and is more compact. Two potential folding pathways, in which two basepairs formed with different order, are observed, and the pathway with the inboard basepair formed before the terminal one is much more favorable, and dominates the folding of the RNA hairpin.

I. Introduction

RNA, one of the fundamental biomolecules for life, plays important roles in gene expression.[1−3] It has been argued that the RNA-based catalysis and information storage system is the first step in the evolution of cellular life.[4] The functional diversity of RNA is highly related to its structural flexibility and adaptability, which motivated the research on the RNA folding and stability.[5,6] On the other hand, RNA folding is more hierarchically organized. The stable secondary structure can exist without the tertiary structure.[7,8] Thus, the folding of the secondary structure motifs of RNA can be studied in the absence of tertiary structure formation. The RNA hairpin, consisting of a double-stranded RNA (dsRNA) stem and a terminal loop, is the most abundant secondary structure of RNA, and is essential to the folding and function of RNA.[9−11] Thus, the RNA hairpin is an ideal model system for understanding the general folding mechanism of RNA molecules.

During the past decades, a number of studies on the folding of the RNA hairpin have been performed both theoretically and experimentally.[9−23] Considerable progress has been made in understanding the mechanism of RNA hairpin folding. However, our knowledge of RNA hairpin folding is still very limited.[8,13] It had been suggested that, in some cases, the folding of an RNA hairpin can be described by a so-called two-state model,[15,19,20] i.e., hopping between the denatured state and the native state without any accumulation of intermediate states, and the folding transition resembles a first-order phase transition. However, some other theoretical studies suggested that the folding of RNA hairpins should be more complex due to the energetic and topological frustration.[13,14] For example, on the basis of the three-interaction-site model, Hyeon and Thirumalai revealed the complicated behaviors for the folding of a 22-nucleotide RNA hairpin.[22] In ref 23, by using the all atom simulations, Bowman and co-workers showed that, even for a 12-nucleotide RNA hairpin, multiple intermediates can exist during the folding.

Recently, the folding of a very small RNA hairpin, which consists of only a tetraloop and a two-basepair stem, has been studied experimentally. Combined with the analysis based on a simple lattice model, the authors showed that a rugged energy landscape, containing four states, was reasonable to describe the folding of this small RNA hairpin.[12] However, the detailed molecular picture of the folding for this small RNA hairpin is still lacking because of the limited time and spatial resolutions in experiment. This RNA hairpin is very small, containing only eight nucleotides. The experimental data on the folding kinetics suggested that it is a fast-folding folder. Thus, it is feasible to simulate the folding of this RNA hairpin by the molecular dynamics at the all atom level. Very recently, Garcia and Paschek investigated the folding of this RNA hairpin based on the replica exchange molecular dynamics (REMD) simulation. They found that, even starting from the extended structure, the RNA hairpin can fold to the native state within reasonable simulation time.[21] They also argued that the folding behavior is complicated. To fully understand the folding mechanism of this small RNA hairpin, more detailed characterization of the folding intermediates and pathways is still needed.

In this work, we present a study on the folding of this 8-mer RNA hairpin with an all atom model based on the REMD simulation.[24,25] We find that the 8-mer RNA hairpin shows a very complicated folding behavior with four different states, instead of a two-state transition mechanism. This result is consistent with experimental observations.[12] These four major states, e.g., the native state, the intermediate state, the unfolded state, and the misfolded state, are categorized on the basis of the formation of the basepairs at the stem and structure similarity of the RNA hairpin. The detailed structures of these major states and their relevance to the folding are also discussed.

II. Model and Methods

The 8-nucleotide RNA hairpin, consisting of a tetraloop and a two-basepair stem with the sequence 5′-gcUUCGgc, has been

* To whom correspondence should be addressed. E-mail: wfli@nju.edu.cn (W.F.L.); wangwei@nju.edu.cn (W.W.).
† Fudan University.
‡ National Laboratory of Solid State Microstructure and Department of Physics, Nanjing University.
§ State Key Lab of Pharmaceutical Biotechnology, Nanjing University.

10.1021/jp904573r
Published on Web 04/14/2010

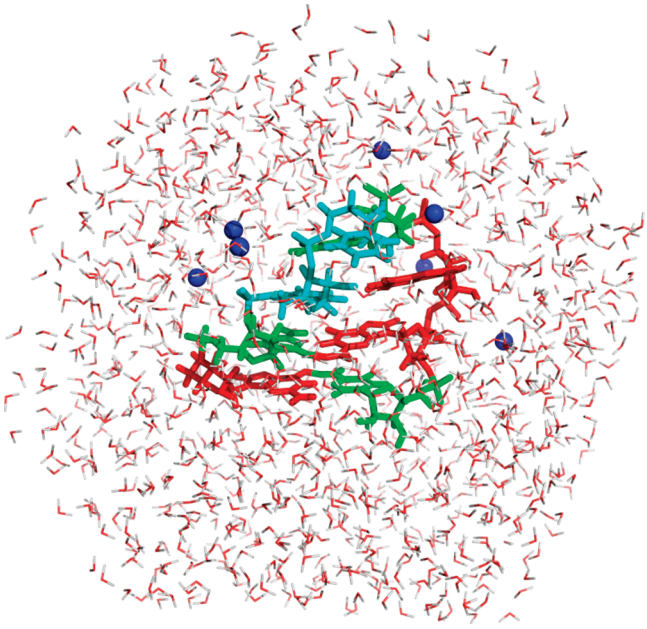

Figure 1. Simulation system of the RNA hairpin. The 8-mer RNA hairpin (the guanine, cytosine, and uracil are colored by red, green, and cyan) is placed in an octahedral water box.

considered to be the smallest RNA which folds into a stable and well-formed hairpin.[12] In our study, this RNA hairpin was modeled by AMBER8 with the ff99 force field and periodic boundary conditions.[26] In the simulation, the small hairpin was placed in a truncated octahedral box containing 1347 TIP3P water molecules. Seven Na^+ ions were added to neutralize the system (see Figure 1). The equation of motion of this molecular dynamics (MD) system was integrated by using the leapfrog algorithm with a time step of 2 fs. Covalent bonds involving the hydrogen atom were constrained by the SHAKE algorithm.[27] The particle-mesh Ewald method (PME)[28] was employed to treat the long-range electrostatic interactions. The nonbonded cutoff was set to 12.0 Å. The X-ray structure (PDB code 1F7Y, truncated to nucleotides 31−38) was used as the initial structure for the simulation. Before the production simulations, the crystal structure is first minimized by 8000 steps. Then, the minimized system is equilibrated in the NTP ensemble to a pressure of 1 atm and a temperature of 298.0 K, which resulted in a box volume of ∼43000 $Å^3$ and a salt concentration of ∼280 mM.

In this work, the conformational sampling is performed by using the REMD which is a high efficiency sampling method and has been widely used in the study of protein folding, aggregation, and other large scale functional motions of biological importance.[21,25,29−36] In the REMD method, a number of independent replicas with different temperatures are simulated in parallel. After a certain time interval, the exchange of replicas between neighboring temperatures is attempted with the probability of successful exchange being determined by the energy and temperature differences of the replica pair based on the Metropolis criterion. Due to the conformational exchange, the conformations at low temperatures have the ability to overcome high energy barriers by switching to higher temperatures, which therefore improves the sampling efficiency. For example, in ref 37, Sanbonmatsu and Garcia compared the sampling efficiencies of the REMD and conventional MD by modeling the peptide Met-enkephalin with explicit solvent. Their results suggested that the REMD samples 5 times more conformational space than the conventional MD. More details on the REMD can be found in refs 24 and 37−39. In this work, a total of 44 replicas are

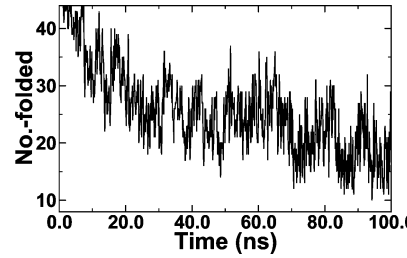

Figure 2. Number of replicas sampling the native state as a function of time. Here, the native state is defined as both basepairs in the stem of the RNA hairpin being formed. A C−G basepair is formed if two of its three hydrogen bonds are formed. The hydrogen bond is considered to be formed if the distance between the donor (D) and acceptor (A) is less than 3.5 Å and the angle D−H−A is larger than 150°.

simulated with the temperatures ranging from 260.0 to 501.0 K. There is no unique way to assign the temperatures for each replica. In this work, before the REMD run, we performed a number of conventional MD for 400 ps in NVT ensembles at temperatures from 260 to 500 K with an interval of 10.0 K. Then, the average potential energy is calculated for each temperature based on the structures sampled during the last 200 ps. The derived average potential energies as a function of temperature are further fitted by a quadratic curve. The temperatures of the REMD simulation are assigned such that the calculated acceptance ratios based on the fitted energy−temperature curve and the Metropolis criterion are constant for all of the replicas. The resulting acceptance ratio varies between 0.16 and 0.18. For each replica, the simulation length is around 100.0 ns, and the structures sampled during the last 50.0 ns are used for data analysis. In addition to the above simulations, we also conducted a conventional MD simulation in the NVT ensemble at 298.0 K for 20 ns to calculate the formation probability of the hydrogen bonds. A hydrogen bond is considered to be formed in the native state if it exists in more than 50% of the sampled structures.

III. Results and Discussion

A. Convergence Verification. Figure 2 shows the number of replicas sampling the native state as a function of time. As we know, the basepairs, including the adenine−uracil basepair (A−U) connected by two hydrogen bonds and the cytosine−guanine basepair (C−G) connected by three hydrogen bonds, play vital roles in the stability of the secondary structure of RNA.[40,41] In the RNA hairpin studied here, there are only two C−G basepairs in its crystal structure. In this work, a structure is considered to be in the native state if both of its basepairs are formed. We noted that the criterion of both basepairs being formed is very strict. Most of the structures with two basepairs have a RMSD less than 4.0 Å, which is the criterion of native structure formation used in the work of Garcia and Pascheck.[21] To demonstrate the sampling quality and the possible convergence, we calculated the average number of the replicas sampling the native state during a time interval of 0.2 ns following the work of ref 21, and the results are shown in Figure 2. We can see that the average number of the replicas sampling the native state decreases with time in the early stage of the simulation, since the simulation is started from the native state. After around 40 ns, it reaches a steady state with around 20 replicas sampling the native state. This result confirms the observation of ref 21, which shows that it took around 50 ns for the system to reach a steady-state starting from the unfolded state. Thus, in the following analysis, the snapshots sampled after the first 50 ns are used.

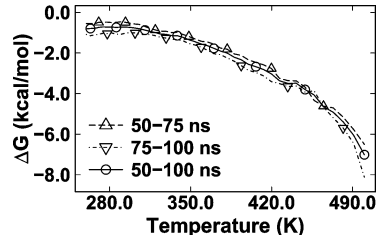

Figure 3. Difference of free energy between the non-native states and the native state as a function of temperature calculated based on the data of the time periods 50−75, 75−100, and 50−100 ns, respectively.

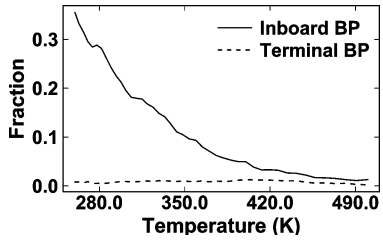

Figure 4. Fractions of two classes of conformations in the intermediate as a function of temperature. There is only one basepair in the conformations of the intermediate.

To further test the reasonable convergence of the simulation, we compared the free energy difference ΔG between the native state and the non-native state sampled during the time periods 50−75, 75−100, and 50−100 ns at different temperatures. Here, the free energy difference is calculated on the basis of the relative papulation of the native state by $\Delta G = -RT \ln[(1 - P_n)/P_n]$, with P_n being the fraction of native structures and R being the gas constant. The results are shown in Figure 3. From Figure 3, one can see that the difference between the three ΔG curves is very small, and the overall behavior is similar to that observed in the work by Garcia and Paschek,[21] which suggests again that a reasonable convergence is achieved. It is worth noting that, in Figure 3, ΔG is negative even at temperatures lower than 300 K, which apparently underestimates the stability of the native state. Such a negative free energy difference was also shown in ref 21, in which a much longer simulation is performed starting from the unfolded state. One possible reason for the observed low stability of the native structure is the difference of the salt concentrations used in the simulations and experiments. It is worth mentioning that, even with the REMD, the absolute convergence is still difficult to achieve within the time scale of 100 ns; thus, the quantitative discussions are still unfeasible in our study. However, we believe that the major states have been well sampled and we can discuss the folding mechanism based on these simulations qualitatively.

B. Intermediate and Folding Pathway. There are two basepairs in the native conformations. Both of them are broken in the unfolded state. Thus, it is natural to suggest that there is an intermediate between the native state and the unfolded state, in which only one basepair is formed. Indeed, a number of one-basepair conformations are observed in our simulations. It is interesting to investigate which basepair is formed in these intermediate conformations, since different basepairs formed in the intermediate imply different pathways for the folding. A statistical survey on the one-basepair conformations is performed. Figure 4 shows the fractions of the conformations with only the inboard basepair or only the terminal basepair formed as a function of the temperature (represented by a solid line and a dashed line, respectively). One can see that the fraction of the conformations with the inboard basepair formed is much higher than that of the conformations with the terminal basepair formed. The fraction of the conformations with only the inboard basepair is higher than 0.30 at lower temperatures. However, it decreases with temperature quickly. In comparison, the fraction of the conformations with only the terminal basepair is lower than 0.02 for all of the temperatures. That is, compared with the conformations with the terminal basepair formed, the conformations with the inboard basepair formed are much more stable. These results indicate that the folding of this small RNA hairpin mostly follows the zipping mechanism.

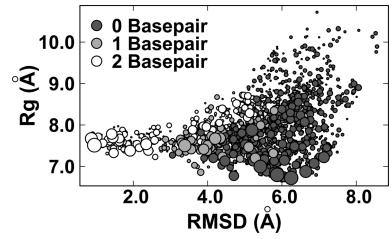

Figure 5. Distribution of the clusters around room temperature. The size of the cluster is denoted by the radius of the circle in logarithm scale. The clusters which contain only one conformation are not shown in this figure, since their radius is zero. The filled gray scale in the circle denotes the number of basepairs in the central conformation of the cluster.

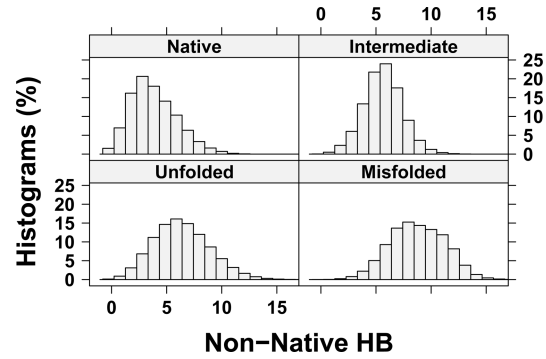

Figure 6. Histogram of the non-native hydrogen bonds for the conformations of the four states. Here, the non-native hydrogen bonds include all of the hydrogen bonds not formed in the native state. A hydrogen bond is considered to be formed in the native state when more than 50% of the structures sampled during a 20 ns relaxation of the native structure at room temperature. There are seven native hydrogen bonds, including six hydrogen bonds of the two C−G basepairs and one hydrogen bond in the loop.

C. Conformational Clusters. Figure 5 shows the conformational clusters around room temperature on the conformational space formed by RMSD from native structure and radius of gyration. Here, the structure clustering is performed on the basis of the similarity of structures measured by RMSD following the algorithm of Daura and co-workers.[42,43] The RMSD cutoff is set to 1.0 Å in the clustering, and all of the non-hydrogen atoms are used in the RMSD fitting. On the basis of the number of basepairs in the central structures of the clusters, all of the clusters are divided into three groups in which the conformations have zero, one, and two native basepairs, respectively. From Figure 5, one can see that the three groups of clusters are almost well separated. The clusters with two basepairs, corresponding to the native conformations, mainly distribute in the region of RMSD < 3.0 Å and 7.2 Å < R_g < 8.0 Å. The clusters with one basepair, corresponding to the intermediate conformations, mainly distribute in the region of 3.0 Å < RMSD < 5.5 Å and 7.4 Å < R_g < 8.2 Å. The most notable clusters in this figure are those without a basepair formed. This group of clusters can be further divided into two

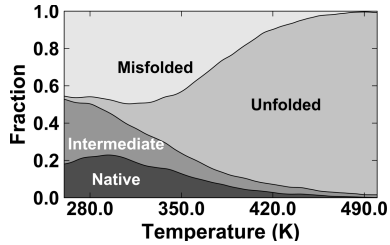

Figure 7. Fractions of conformations as a function of temperature. Here, all of the conformations have been categorized into four major states, and the width of an area in vertical at a certain temperature denotes the fraction of the state.

categories, namely, those with large values of R_g and those with small values of R_g. The clusters with large values of R_g can be considered as unfolded conformations, since they are relatively extended, and have a small cluster size. However, for the clusters with small values of R_g, they have relatively large cluster size. For example, the most compact cluster without a basepair formed in this figure contains 1958 structures, which is the second biggest cluster in this figure and only smaller than a native conformational cluster. This result means that this group of clusters is relatively stable, even more stable than the intermediate conformations. Meanwhile, these clusters are very compact. The values of R_g of these clusters are similar to, even smaller than, that of the native conformations. These clusters are observed in many trajectories, especially at low temperatures. It may play important roles during the folding of the RNA hairpin. More detailed analysis reveals that, in these clusters, a number of non-native hydrogen bonds are formed (see Figure 6). Since the non-native hydrogen bonds need to be broken in order to fold to the native conformation, we assign the collection of these clusters as the misfolded state. Such observation of the misfolded state is consistent with the folding picture proposed by Ma and co-workers in which they found that an off-pathway intermediate is necessary to explain the experimental observations based on a two-dimensional lattice model.[12] Therefore, there are four major states in the folding of the RNA hairpin, i.e., the native state, the intermediate state, the unfolded state, and the misfolded state. It is worth emphasizing that here the misfolded state represents an ensemble of diverse conformations, since the differences between the conformations in this state are very significant, and there may be no direct transitions between these conformations.

D. Four-State Model. Figure 7 shows the fractions of conformations at different temperatures for the four major states. In classifying conformations, the number of the basepairs is used preferentially. When both basepairs are formed in a conformation, it is categorized into the native state. When there is only one basepair in the conformation, it is categorized into the intermediate. The conformations without a basepair are clustered by their similarity. If a cluster contains more than 10 structures, it is considered to be a misfolded cluster. Otherwise, it is classified as the unfolded cluster, since the misfolded conformations are more stable and can maintain a long time in the simulation. As shown in Figure 7, the folding of the RNA hairpin has low cooperativity, and the fractions of the four major states change with temperature smoothly. In detail, the fraction of the native state is maintained at 0.20 when the temperature is lower than 310 K. When temperature is higher than 310 K, the fraction of the native state decreases with temperature. Such a temperature dependence of the fraction of native state is consistent with the experimentally observed melting curve (Figure 2 in ref 12). However, in the experimental melting curve, the fraction of the folded state is around 1.0 at low temperatures which is much higher than the present simulation results. Meanwhile, at temperatures of around 360 K, the RNA hairpin is almost unfolded. In comparison, in our simulated results, up to the temperatures around 400 K, the folded structure still has significant populations. Such a difference may result from the different definition of the folded state in experiment and simulation. For example, in experiment, it is not easy to unambiguously differentiate the native state from the misfolded state and the intermediate observed in this work. The accuracy of the force field and the difference of the salt concentration may also contribute to such discrepancy, as mentioned in the beginning of this section. The intermediate is most sensitive to the temperature. As the temperature increases from 260 to 360 K, the fraction of the intermediate decreases from 0.35 to less than 0.10. The fraction of the misfolded state is maintained at ~0.45

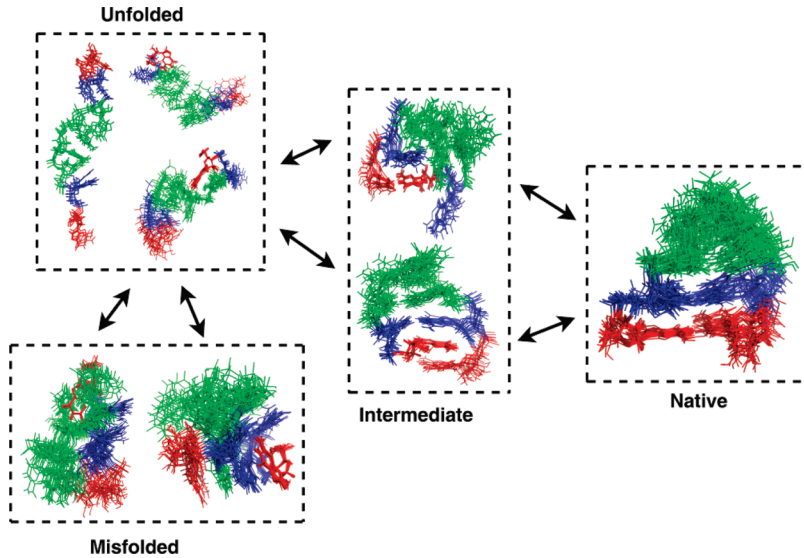

Figure 8. Schematic plots for the folding pathway of the RNA hairpin. Here, the four states are represented by the representative conformations of the corresponding states. The arrow lines denote the pathways between these states. The colors indicate the loci of the nucleotides in the native structure: red for the terminal basepair, blue for the inboard basepair, and green for the tetraloop.

until the temperature is higher than 350 K, and then decreases with temperature. For temperatures higher than 360 K, the unfolded state is the dominant state.

E. Folding Pathway. The above results show that the folding of the RNA hairpin is very complex though its structure is very simple. Four major states have been observed in the folding of this RNA hairpin. On the basis of the structural characteristics of these four major states, we suggest a folding scenario in which two folding pathways are possible. These two pathways differ by the formation sequence of the inboard basepair and the terminal basepair. For the misfolded state, it is compact and without basepair formed, while there are many non-native hydrogen bonds in their conformations. To form the native conformation, these non-native hydrogen bonds should be broken at first. This state may correspond to the off-pathway intermediate raised by Ma and co-workers to explain the experimental observation.[12] As a summary of the folding mechanism of the RNA hairpin, Figure 8 shows the folding pathways of this RNA hairpin. In this figure, the state is represented by some representative structures, and the transitions between the major states are denoted by the arrow lines. It is worth noting that the kinetic information is lost in REMD due to the inherent discontinuity of the REMD trajectories.[24,25] The folding pathways shown here are based on the progression along reaction coordinates and conformations of the states, instead of time. To fully follow the folding pathway corresponding to the time sequence, long time-scale simulations with the conventional MD are needed.

IV. Conclusion

In this work, the folding of an 8-nucleotide RNA hairpin has been studied at the all atom level based on the REMD. A very complicated folding landscape is revealed, consistent with the experimental observations and other computational studies. According to the number of basepairs and the similarity of the conformations, four major states were identified in the folding of this small RNA hairpin, i.e., the native state, the intermediate state, the unfolded state, and the misfolded state. The transitions between these states are proposed on the basis of the progression along reaction coordinates and conformations of these states. It was found that the conformations of the native state, which are similar to the crystal structure, contain two basepairs. In the folding transition, there are two potential folding pathways, in which the two basepairs form in different order. Among them, the pathway with the inboard basepair formed first is much more dominant, and the pathway with the terminal basepair formed first only has a minor population, indicating that the zipping mechanism is the favorable pathway for the folding of the RNA hairpin. The misfolded state, which is off-pathway, has a very high population in the simulations. The non-native hydrogen bonds have an important contribution to the stabilization of this misfolded state. We believe that our results are helpful to understand the folding mechanism of the RNA hairpin, as well as the conformational change of RNA.

Acknowledgment. We are thankful for the helpful discussions with Prof. Jun Wang. This research is supported in part by the Major Program of National Natural Science Foundation of China (Program of Protein) under Grant No. 10834002, the National Basic Research Program of China (973 Program) under Grant No. 2007CB814800, the National Natural Science Foundation of China under Grant Nos. 10704033 and 10834002, the Program of Jiangsu Provice, China under Grant No. BK2009008, Shanghai Leading Academic Discipline Project under Grant No. B111, and Shanghai Supercomputer Center of China.

References and Notes

(1) Fire, A. Z. *Angew. Chem., Int. Ed.* **2007**, *46*, 6966–6984.
(2) Kornberg, R. *Angew. Chem., Int. Ed.* **2007**, *46*, 6956–6965.
(3) Mello, C. C. *Angew. Chem., Int. Ed.* **2007**, *46*, 6985–6994.
(4) Gesteland, R. F.; Cech, T.; Atkins, J. F. *The RNA world: the nature of modern RNA suggests a prebiotic RNA world*; Cold Spring Harbor Laboratory Press: 2006.
(5) Herschlag, D. *J. Biol. Chem.* **1995**, *270*, 20871–20874.
(6) Schroeder, R.; Barta, A.; Semrad, K. *Nat. Rev. Mol. Cell Biol.* **2004**, *5*, 908–919.
(7) Brion, P.; Westhof, E. *Annu. Rev. Biophys. Biomol. Struct.* **1997**, *26*, 113–137.
(8) Onoa, B.; Tinoco, I. J. *Curr. Opin. Struct. Biol.* **2004**, *14*, 374–379.
(9) Svoboda, P.; Cara, A. D. *Cell. Mol. Life Sci.* **2006**, *63*, 901–918.
(10) Noller, H. F. *Science* **2005**, *309*, 1508–1514.
(11) Pljevaljčić, G.; Millar, D. P.; Deniz, A. A. *Biophys. J.* **2004**, *87*, 457–467.
(12) Ma, H. R.; Proctor, D. J.; Kierzek, E.; Kierzek, R.; Bevilacqua, P. C.; Gruebele, M. *J. Am. Chem. Soc.* **2006**, *128*, 1523–1530.
(13) Zhang, W. B.; Chen, S. J. *Biophys. J.* **2006**, *90*, 765–777.
(14) Zhang, W. B.; Chen, S. J. *Biophys. J.* **2006**, *90*, 778–787.
(15) Hyeon, C.; Thirumalai, D. *Proc. Natl. Acad. Sci. U.S.A.* **2005**, *102*, 6789–6794.
(16) Bundschuh, R.; Gerland, U. *Phys. Rev. Lett.* **2005**, *95*, 208104.
(17) Draper, D. E. *RNA* **2004**, *10*, 335–343.
(18) Thirumalai, D.; Hyeon, C. *Biochemistry* **2005**, *44*, 4957–4970.
(19) Bonnet, G.; Krichevsky, O.; Libchaber, A. *Proc. Natl. Acad. Sci. U.S.A.* **1998**, *95*, 8602–8606.
(20) Liphardt, J.; Onoa, B.; Smith, S. B.; Tinoco, I., Jr.; Bustamante, C. *Science* **2001**, *292*, 733–737.
(21) Garcia, A. E.; Paschek, D. *J. Am. Chem. Soc.* **2008**, *130*, 815–817.
(22) Hyeon, C.; Thirumalai, D. *J. Am. Chem. Soc.* **2008**, *130*, 1538–1539.
(23) Bowman, G. R.; Huang, X.; Yao, Y.; Sun, J.; Carlsson, G.; Guibas, L. J.; Pande, V. S. *J. Am. Chem. Soc.* **2008**, *130*, 9676–9678.
(24) Sugita, Y.; Okamoto, Y. *Chem. Phys. Lett.* **1999**, *314*, 141–151.
(25) Zhou, R. *J. Mol. Graphics Modell.* **2004**, *22*, 451–463.
(26) Case, D. A.; Pearlman, D. A.; Caldwell, J. W.; Cheatham, T. E., III; Wang, J.; Ross, W. S.; Simmerling, C. L.; Darden, T. A.; Merz, K. M.; Stanton, R. V.; Cheng, A. L.; Vincent, J. J.; Crowley, M.; Tsui, V.; Gohlke, H.; Radmer, R. J.; Duan, Y.; Pitera, J.; Massova, I.; Seibel, G. L.; C., S. U.; Weiner, P. K.; Kollman, P. A. *Amber 8 manual*; University of California: San Francisco, CA, 2004 (amber.scripps.edu).
(27) Ryckaert, J. P.; Cicotti, G.; Berendsen, H. J. C. *J. Comput. Phys.* **1993**, *23*, 327–341.
(28) Darden, T.; York, D.; Petersen, L. *J. Chem. Phys.* **1993**, *98*, 10089–10092.
(29) Li, W. F.; Zhang, J.; Wang, J.; Wang, W. *J. Am. Chem. Soc.* **2008**, *130*, 892–900.
(30) Garcia, A. E.; Onuchic, J. N. *Proc. Natl. Acad. Sci. U.S.A.* **2003**, *100*, 13898–13903.
(31) Zhou, R. H. *Methods Mol. Biol.* **2007**, *350*, 205–223.
(32) Zhou, R. H. *Proc. Natl. Acad. Sci. U.S.A.* **2003**, *100*, 13280–13285.
(33) Zhou, R. H.; Berne, B. J. *Proc. Natl. Acad. Sci. U.S.A.* **2002**, *99*, 12777–12782.
(34) Zhang, J.; Li, W. F.; Wang, J.; Qin, M.; Wang, W. *Proteins* **2008**, *72*, 1038–1047.
(35) Ahmad, M.; Gu, W.; Helms, V. *Angew. Chem., Int. Ed. Engl.* **2008**, *47*, 7626–7630.
(36) Nymeyer, H.; Garcia, A. *Proc. Natl. Acad. Sci. U.S.A.* **2003**, *100*, 13934–13939.
(37) Sanbonmatsu, K. Y.; Garcia, A. E. *Proteins* **2002**, *46*, 225–234.
(38) Mitsutake, A.; Sugita, Y.; Okamoto, Y. *Biopolymers* **2001**, *60*, 96–123.
(39) Zhang, W.; Wu, C.; Duan, Y. *J. Chem. Phys.* **2005**, *123*, 154105.
(40) Dittmer, J.; Kim, C. H.; Bodenhausen, G. *J. Biomol. NMR* **2003**, *26*, 259–275.
(41) Markley, G.; Bax, L.; Arata, Y.; Hilbers, C. W.; Kaptein, R.; Sykes, B. D.; Wright, P. E.; Wüthrich, K. *J. Mol. Biol.* **1998**, *280*, 933–952.
(42) van der Spoel, D.; Lindahl, E.; Hess, B.; van Buuren, A. R.; Apol, E.; Meulenhoff, P. J.; Tieleman, D. P.; Sijbers, A. L. T. M.; Feenstra, K. A.; van Drunen, R.; Berendsen, H. J. C. Gromacs user manual version 3.3, 2005 (www.gromacs.org).
(43) Daura, X.; Gademann, K.; Jaun, B.; Seebach, D.; van Gunsteren, W. F.; Mark, A. E. *Angew. Chem., Int. Ed.* **1999**, *38*, 236–240.

JP904573R